International Journal of Engineering Science 133 (2018) 336–351

Contents lists available at ScienceDirect

International Journal of Engineering Science

journal homepage: www.elsevier.com/locate/ijengsci

Torsional deformations and material tailoring of orthotropic bi-directional FGM hollow truncated conical cylinders with curved lateral surfaces

R.C. Batra [a,*], G.J. Nie [b,a]

[a] Department of Biomedical Engineering and Mechanics, Virginia Polytechnic Institute and State University, Blacksburg, VA 24061, USA
[b] School of Aerospace Engineering and Applied Mechanics, Tongji University, Shanghai 200092, China

ARTICLE INFO

Article history:
Received 11 September 2018
Revised 29 September 2018
Accepted 8 October 2018

Keywords:
Material tailoring
Orthotropic bi-directional functionally graded materials
Hollow truncated conical cylinders
Curved bounding surfaces

ABSTRACT

Converging and diverging nozzles and skyscrapers are examples of hollow structures with curved bounding surfaces. We study torsional deformations of such structures, namely, truncated conical cylinders with curved inner and outer bounding surfaces and made of linearly elastic and orthotropic functionally graded materials (FGMs). Simplifying assumptions include a plane section remains plane, deformations are axisymmetric about the cylinder axis, and a power-law relation between the radial and the axial coordinates describes the curved mantle. For four spatial variations of the two shear moduli, we analytically solve governing equations for the two non-zero shear stresses and the tangential displacement. For a general variation of the shear moduli we employ the weighted residuals approach to find an approximate solution and establish its convergence and accuracy. We also analyze the material tailoring problem to attain a desired shear stress distribution on a cross-section. We include numerical examples to illustrate spatial distributions of shear stresses for prescribed shear moduli variations, and of the shear moduli for achieving desired shear stress distributions. The analytical solutions provided herein should serve as benchmarks to verify numerical solutions of similar problems.

1. Introduction

Functionally graded materials (FGMs) are inhomogeneous and have continuously varying material properties in one or more space dimensions usually obtained by continuously varying volume fractions of constituents. Thus, one can effectively reduce interlaminar delaminations, stress concentrations at interfaces between two distinct materials, and exploit advantageous properties of constituents. For example, alumina/metal FGMs take advantage of high thermal resistance of alumina and superior tensile strength of the metal. Whereas researchers have been analyzing deformations and stresses in linearly elastic inhomogeneous materials since 1960s, there has been accelerated activity during the last two decades as evidenced by the number of papers published in the open literature (Birman & Byrd, 2007; Gupta & Talha, 2015; Jamshidi & Arghavani, 2018; Lieu & Lee, 2017; Nedin, Vatulyan, & Bogachev, 2018; Roque & Martins, 2015; Swaminathan & Sangeetha, 2017; Wetherhold, Seelman, & Wang, 1996). We note that a nonlinear problem for an inhomogeneous cylinder was numerically analyzed by Batra in 1980 (Batra, 1980).

* Corresponding author.
E-mail address: rbatra@vt.edu (R.C. Batra).

https://doi.org/10.1016/j.ijengsci.2018.10.001
0020-7225/

Initial-boundary-value problems for structures composed of linearly elastic FGMs are challenging because coefficients in governing equations depend upon the spatial coordinates, except when all properties vary exponentially with the same exponent. Even though mathematically attractive, it is nearly impossible to achieve the same spatial variation for all material moduli and the mass density. Solutions for several static problems involving linearly elastic FGMs are given in Lekhnitskii's book (Lekhnitskii, 1981). In order to limit the article length, we do not cite all FGM related works.

Chen (1964), Rooney and Ferrari (1995), and Horgan and Chan (1999), among others, have provided analytical solutions for torsional deformations of circular cylindrical FGM bars by assuming the shear modulus to vary smoothly in a cross-section. They found that the maximum shear stress does not, in general, occur on the rod boundary, in contrast to that for a homogeneous material bar. For torsional deformations of FGM tubes of arbitrary cross-section, Arghavan and Hematiyan (2009), Ecsedi (2009, 2013), and Chen (2011) have provided analytical solutions under the assumption of the shear modulus continuously varying in the radial direction.

Considering that the analytical solutions are possible under special circumstances, some researchers, e.g., Jog and Mokashi (2014), Katsikadelis and Tsiatas (2016), numerically solved torsional problems for anisotropic FGM non-circular prismatic bars, respectively, by the finite element and the boundary element methods (FEM/BEM).

Lekhnitskii (1981) has analytically analyzed torsional deformations of a truncated conical cylinder with straight sides and the shear moduli varying along both the radial and the axial directions according to either power-law functions of r and z or power-law functions of r/z. Here (r, θ, z) denote coordinates of a point in the cylindrical coordinate system with the origin at the cone vertex. Nie, Pydah, and Batra (2018) have provided analytical solutions for a few spatial variations of the shear modulus, and have numerically solved problems by using the Weighted Residuals Approach (WRA). Here we extend the work to conical orthotropic FGM cylinders with lateral surfaces described by a power-law relation between r and z, and material moduli varying in the axial and the radial directions. We provide analytical solutions for a few spatial variations of the shear moduli, and numerical solutions for other cases. In general, in the FEM, one replaces a curved boundary by a polygonal one that can have stress concentrations at vertices/corners. The WRA overcomes this at the cost of using non-simple basis functions that require either analytical integrations or a large number of quadrature points to numerically evaluate the integrals. The WRA is simpler than the traditional FEM.

Material tailoring problems, i.e., finding spatial variations of the material moduli to achieve a prescribed stress state, are more challenging than the stress analysis problems. Lekhnitskii (1962) has derived conditions that Young's modulus and Poisson's ratio must satisfy to achieve a desired radial distribution of stresses in a wedge and a half-plane. For plane strain axisymmetric deformations of an orthotropic FGM cylinder, Leissa and Vagins (1978) assumed that all material moduli are proportional to each other and found their spatial variation to make either the hoop stress or the maximum in-plane shear stress uniform in the cylinder. By assuming that the volume fraction of phases to change only radially, Tanaka, Watanabe, Sugano, and Poterasuc (1996) investigated material tailoring of a FGM hollow cylinder to globally reduce thermal stresses by using the direct sensitivity analysis, multi-objective optimization and the incremental FEM. Similarly, Ootao, Kawamura, Tanigawa, and Imamura (1999), Ootao, Tanigawa, and Ishimaru (2000), and Cho and Ha (2002a, 2002b) optimized material composition of FGM plates and hollow spheres to minimize thermal stresses by using either a genetic algorithm, or an artificial neural network, or an interior penalty-function method. Na and Kim (2009a, 2009b, 2010) assumed material properties to be temperature dependent, and numerically optimized volume fractions of constituents for FGM panels to reduce stresses and improve thermo-mechanical buckling behavior. Liaghat, Hematiyan, and Khosravifard (2014) have numerically tailored volume fractions of constituents in torsional deformations of FGM hollow rods to achieve either an arbitrary distribution of the shear stress over a rod cross section or the maximum torsional rigidity for a constant mass. Shabana, Elsawaf, Khalaf, and Khalil (2017) and Wang, Dong, and Atluri (2018) employed the particle swarm optimization technique to minimize stresses in FGM cylinders. Batra (2006) has shown that the angle of twist per unit length can be controlled by smoothly varying the shear modulus in the axial direction in a FGM circular cylinder.

Multi-objective optimization of FGM structures has been studied by Goupee and Vel (2007), Huang, Fadel, Blouin, and Grujicic (2002), Vel and Pelletier (2007) and Correia, Madeira, Araújo, and Soares (2018). We note that optimal designs are problem-dependent as should be evident from the closed-form solutions provided by Batra (2011, 2015), Dryden and Batra (2013a, 2013b), Nie and Batra (2010a, 2010b, 2010c) and Nie, Zhong, and Batra (2011). As far as we can ascertain, the material tailoring problem for a hollow conical cylinder with curved lateral surfaces has not been studied.

Here we first formulate the boundary-value problem for a linearly elastic and orthotropic FGM hollow truncated conical cylinder with curved lateral surfaces. We then analytically analyze stresses and displacements for a few spatial variations of the two shear moduli in a cylinder with straight lateral surfaces. Subsequently, we use the WRA to numerically solve boundary-value problems for a cylinder with curved lateral surfaces. Finally, we tailor the shear moduli to attain a pre-specified variation of two shear stresses in a cylinder.

The analytical results should serve as benchmarks for verifying numerical solutions of problems similar to those studied herein.

2. Problem formulation

As schematically shown in Fig. 1, we analyze static deformations of a linearly elastic FGM hollow truncated conical cylinder with curved inner and outer lateral surfaces defined by the power-law relations

$$R_z^i = \beta_1 z^p, \tag{1a}$$

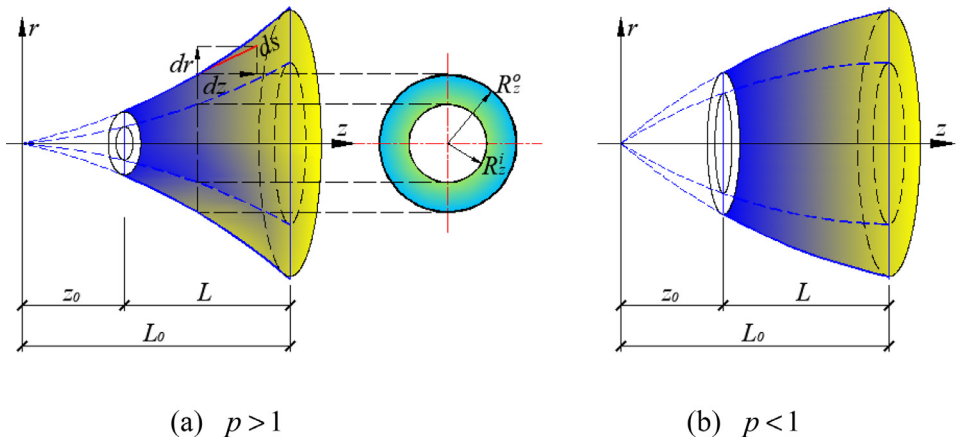

Fig. 1. Schematic sketch of a FGM hollow truncated conical cylinder with curved lateral surfaces.

$$R_z^o = \beta_2 z^p \tag{1b}$$

where R_z^i and R_z^o, respectively, denote the inner and the outer radii of a cross-section $z = c$, a constant. Constants β_1, β_2 and p define the lateral surfaces. For $p = 1$, the two lateral surfaces are straight, and $\beta_1 = \tan\alpha_i$ and $\beta_2 = \tan\alpha_o$, where α_i and α_o, respectively, equal the half opening angles of the inner and the outer surfaces of the cylinder.

The cylinder is deformed by applying equal and opposite torques at the end faces, $z = z_0$ and L_0. The two lateral surfaces of the cylinder are traction free, and the resultant axial force on end faces, $z = z_0$, L_0 equals zero. We assume that the variation of material properties in the r- and the z-directions is such that the cylinder deformations are axisymmetric and a plane section $z =$ constant remains plane. Thus, only tangential or circumferential displacement, u_θ, is non-zero and it depends upon r and z.

For infinitesimal deformations, strains ε_r, ε_θ, ε_z, $\gamma_{\theta z}$, γ_{zr}, and $\gamma_{r\theta}$ are related as follows to u_θ.

$$\varepsilon_r = 0, \varepsilon_\theta = 0, \varepsilon_z = 0, \gamma_{\theta z} = \frac{\partial u_\theta}{\partial z}, \gamma_{zr} = 0, \gamma_{r\theta} = \frac{\partial u_\theta}{\partial r} - \frac{u_\theta}{r} \tag{2}$$

We assume that the FGM is linearly elastic and orthotropic with the material principal axes coincident with the cylindrical coordinate axes, (r, θ, z). Thus stresses at a point are related to strains and hence displacements as

$$\sigma_r = \sigma_\theta = \sigma_z = \tau_{zr} = 0, \tau_{\theta z} = G_{\theta z}(r,z)\frac{\partial u_\theta}{\partial z}, \tau_{r\theta} = G_{r\theta}(r,z)\left(\frac{\partial u_\theta}{\partial r} - \frac{u_\theta}{r}\right) \tag{3}$$

where the shear moduli $G_{\theta z}(r, z)$ and $G_{r\theta}(r, z)$ are assumed to have positive values at every point of the cylinder.

Substituting from Eq. (3) into the three equilibrium equations shows that two of them are identically satisfied, and the third, in the absence of body forces, is

$$\frac{\partial \tau_{r\theta}}{\partial r} + \frac{\partial \tau_{\theta z}}{\partial z} + \frac{2\tau_{r\theta}}{r} = 0 \tag{4}$$

The boundary conditions of null tractions on the cylinder lateral surfaces require that

$$-\tau_{\theta z}\frac{dr}{ds} + \tau_{r\theta}\frac{dz}{ds} = 0 \tag{5}$$

where ds is the arc length shown in Fig. 1(a). Recalling Eqs. (1a) and (1b), boundary conditions (5) on the inner and the outer lateral surfaces, respectively, can be written as

$$\tau_{r\theta} = \beta_1 p z^{p-1}\tau_{\theta z}, \tag{6a}$$

$$\tau_{r\theta} = \beta_2 p z^{p-1}\tau_{\theta z} \tag{6b}$$

The boundary conditions on the end faces, $z = z_0$ and L_0, are

$$\int_{R_z^i}^{R_z^o} \tau_{\theta z} r^2 dr = \frac{M_t}{2\pi}, \int_{R_z^i}^{R_z^o} \tau_{\theta z} r dr = 0 \tag{7}$$

where M_t is the applied twisting moment. We note that the tangential traction, $\tau_{\theta z}$, is not point-wise prescribed.

Airy stress function

In terms of the Airy stress function, $\phi(r, z)$, non-zero stress components in Eq. (3) can be expressed as

$$\tau_{\theta z} = \frac{1}{r^2}\frac{\partial \phi(r,z)}{\partial r},\ \ \tau_{r\theta} = -\frac{1}{r^2}\frac{\partial \phi(r,z)}{\partial z} \tag{8}$$

The equilibrium Eq. (4) is identically satisfied, and using Eqs. (3) and (8), we get

$$\frac{\partial}{\partial r}\left(\frac{u_\theta}{r}\right) = -\frac{1}{G_{r\theta}(r,z)r^3}\frac{\partial \phi(r,z)}{\partial z},\ \frac{\partial}{\partial z}\left(\frac{u_\theta}{r}\right) = \frac{1}{G_{\theta z}(r,z)r^3}\frac{\partial \phi(r,z)}{\partial r} \tag{9}$$

Thus, functions $G_{r\theta}(r, z)$, $G_{\theta z}(r, z)$ and $\phi(r, z)$ must satisfy the following compatibility condition

$$\frac{\partial}{\partial r}\left[\frac{1}{r^3 G_{\theta z}(r,z)}\frac{\partial \phi}{\partial r}\right] + \frac{1}{r^3}\frac{\partial}{\partial z}\left[\frac{1}{G_{r\theta}(r,z)}\frac{\partial \phi}{\partial z}\right] = 0 \tag{10}$$

For a given variation of the two shear moduli the Airy stress function can be obtained by solving Eq. (10). Conversely, for prescribed (or desired) spatial distributions of $\tau_{r\theta}$ and $\tau_{\theta z}$ satisfying Eqs. (4), (5) and (7), we can find the two shear moduli, not necessarily uniquely, satisfying Eq. (10) for the material tailoring problem. For an isotropic material, $G_{\theta z}(r, z) = G_{r\theta}(r, z)$ can be determined from Eq. (10).

Introducing the following non-dimensional parameters,

$$R = \frac{r}{L_0},\ Z = \frac{z}{L_0} \tag{11}$$

where $L_0 = L + z_0$, Eq. (10) becomes

$$\frac{\partial}{\partial R}\left[\frac{1}{R^3 G_{\theta z}(R,Z)}\frac{\partial \phi}{\partial R}\right] + \frac{1}{R^3}\frac{\partial}{\partial Z}\left[\frac{1}{G_{r\theta}(R,Z)}\frac{\partial \phi}{\partial Z}\right] = 0 \tag{12}$$

Substitution from Eq. (8) into Eqs. (6a) and (6b) motivates the assumption that $\phi(r, z)$ be a function of $s = r/z^p$. The non-dimensional variable $t = r/z = R/Z$ facilitates solving the problem especially for $p = 1$, i.e., a conical cylinder with straight lateral surfaces.

When the stress function and the two shear moduli depend upon R and Z through t, the compatibility Eq. (12) becomes

$$\left[t^2 G_{\theta z}(t) + G_{r\theta}(t)\right]\frac{\partial^2 \phi}{\partial t^2} - \left[\frac{t^2 G_{\theta z}(t)}{G_{r\theta}(t)}\frac{\partial G_{r\theta}(t)}{\partial t} + \frac{G_{r\theta}(t)}{G_{\theta z}(t)}\frac{\partial G_{\theta z}(t)}{\partial t} + \frac{3G_{r\theta}(t)}{t} - 2tG_{\theta z}(t)\right]\frac{\partial \phi}{\partial t} = 0 \tag{13}$$

Eq. (13) when written using the variable, s, involves the exponent, p, describing the lateral surfaces and is not written here.

3. Solutions for stresses and the displacement

In this Section, we first find exact solutions for a FGM conical cylinder with straight lateral surfaces and the shear moduli having four specific variations with R and Z. Subsequently, problems for a cylinder with curved lateral surfaces and the shear moduli arbitrary functions of R and Z are numerically solved by using the WRA method.

3.1. Exact solutions for FGM conical cylinders with straight lateral surfaces

We assume that the two shear moduli are special functions of coordinates, R and Z. Following Lekhnitskii (1981), we give solutions for the shear moduli *variations* 1 and 2, and provide exact solutions for *new variations* 3 and 4 not investigated by Lekhnitskii (1981) and Nie et al. (2018). For each one of the four variations considered, $G_{\theta z}(R, Z)/G_{r\theta}(R, Z) =$ constant, i.e., the ratio of the two shear moduli at every point equals the same constant.

Variation 1: $G_{\theta z}(R, Z) = g^0_{\theta z} t^n$, $G_{r\theta}(R, Z) = g^0_{r\theta} t^n$

The shear moduli are assumed to have the variations,

$$G_{\theta z}(R,Z) = g^0_{\theta z} t^n,\ \ G_{r\theta}(R,Z) = g^0_{r\theta} t^n \tag{14}$$

where n is an integer, and $g^0_{\theta z}$ and $g^0_{r\theta}$ are reference values of the shear moduli at $t = 1$. Substitution from Eq. (14) into Eq. (13) we find the solution of the resulting equation as

$$\phi = \frac{C_0 t^{n+2}}{n+2}\left[{}_2F_1\left(\frac{3}{2}, 1+\frac{n}{2}; 2+\frac{n}{2}; -\frac{g^0_{\theta z} t^2}{g^0_{r\theta}}\right) - {}_2F_1\left(\frac{5}{2}, 1+\frac{n}{2}; 2+\frac{n}{2}; -\frac{g^0_{\theta z} t^2}{g^0_{r\theta}}\right)\right] \text{ for } n \neq -2 \tag{15a}$$

$$\phi = \frac{C_0}{\left(g^0_{r\theta} + g^0_{\theta z} t^2\right)^{3/2}} \text{ for } n = -2 \tag{15b}$$

where ${}_2F_1(a,b;c;z)=\sum_{k=0}^{\infty}(a)_k(b)_k/(c)_k z^k/k!$ is a hypergeometric function, $(a)_k=\Gamma(a+k)/\Gamma(a)$ is the Pochhammer parameter, and $\Gamma(a)$ is the Gamma function. The constant C_0, found from Eq. (7), has a long expression that is omitted. Eqs. (15a), (15b), (8) and (9) give the following expressions for stresses and the tangential displacement.

For $n\neq -2$

$$\tau_{\theta z}=\frac{1}{L_0^3R^3}\frac{C_0 g^0_{\theta z}(g^0_{r\theta})^{3/2}t^{n+4}}{(g^0_{r\theta}+g^0_{\theta z}t^2)^{5/2}},\ \tau_{r\theta}=\tau_{\theta z}t, \tag{16a}$$

$$u_\theta=-\frac{C_0\sqrt{g^0_{r\theta}}t}{3L_0^2Z^2}\left[\frac{1}{(g^0_{r\theta}+g^0_{\theta z}t^2)^{3/2}}-\frac{1}{(g^0_{r\theta}(Z_0/Z)^2+g^0_{\theta z}t^2)^{3/2}}\right], \tag{16b}$$

and for $n=-2$,

$$\tau_{\theta z}=-\frac{1}{L_0^3R^3}\frac{3C_0 g^0_{\theta z}t^2}{(g^0_{r\theta}+g^0_{\theta z}t^2)^{5/2}},\ \tau_{r\theta}=\tau_{\theta z}t, \tag{17a}$$

$$u_\theta=\frac{C_0 t}{g^0_{r\theta}L_0^2Z^2}\left[\frac{1}{(g^0_{r\theta}+g^0_{\theta z}t^2)^{3/2}}-\frac{1}{(g^0_{r\theta}(Z_0/Z)^2+g^0_{\theta z}t^2)^{3/2}}\right]. \tag{17b}$$

In deriving expressions (16b) and (17b), we have eliminated the rigid body motion of the cylinder by setting $u_\theta(R,Z_0)=0$, i.e., the shorter end face is rigidly clamped.

Variation 2: $G_{\theta z}(R,Z)=g^0_{\theta z}R^{k_1}Z^{k_2}$, $G_{r\theta}(R,Z)=g^0_{r\theta}R^{k_1}Z^{k_2}$

The shear moduli are assumed to be given by

$$G_{\theta z}(R,Z)=g^0_{\theta z}R^{k_1}Z^{k_2},\ G_{r\theta}(R,Z)=g^0_{r\theta}R^{k_1}Z^{k_2}, \tag{18}$$

where $k_1\neq 6$ and k_2 are integers. Eqs. (12) and (18) have the solution

$$\phi=C_0t^{k_1+4}(g^0_{r\theta}+g^0_{\theta z}t^2)^{-\frac{1}{2}(k_1+k_2+3)}\,{}_2F_1\left(1,\frac{1-k_2}{2};\frac{k_1+6}{2};-\frac{g^0_{\theta z}t^2}{g^0_{r\theta}}\right), \tag{19}$$

where constant C_0 can be found from Eq. (7). Proceeding as in the previous case, we obtain expressions for stresses and the displacement as,

$$\tau_{\theta z}=\frac{C_0}{L_0^3R^3}t^{k_1+4}(g^0_{r\theta}+g^0_{\theta z}t^2)^{-\frac{1}{2}(k_1+k_2+3)}[F_1(t)+F_2(t)],\ \tau_{r\theta}=\tau_{\theta z}t, \tag{20}$$

$$u_\theta=\frac{1}{g^0_{\theta z}L_0^2R^{k_1+2}}\int\left(\frac{1}{Z^{k_2+1}}\frac{d\phi}{dt}\right)dZ+C_1(R), \tag{21}$$

where

$$\begin{aligned}F_1(t)&=\frac{g^0_{r\theta}(k_1+4)-g^0_{\theta z}(k_2-1)t^2}{g^0_{r\theta}+g^0_{\theta z}t^2}\,{}_2F_1\left(1,\frac{1-k_2}{2};\frac{k_1+6}{2};-\frac{g^0_{\theta z}t^2}{g^0_{r\theta}}\right),\\ F_2(t)&=\frac{2g^0_{\theta z}(k_2-1)t^2}{g^0_{r\theta}(k_1+6)}\,{}_2F_1\left(2,\frac{3-k_2}{2};\frac{k_1+8}{2};-\frac{g^0_{\theta z}t^2}{g^0_{r\theta}}\right),\end{aligned} \tag{22}$$

and $C_1(R)$ can be found by requiring that $u_\theta(R,Z_0)=0$. The integral in Eq. (21) can be evaluated for a known value of the integer k_2.

Variation 3: $G_{\theta z}(R,Z)=g^0_{\theta z}(\frac{R^{k-2}}{Z^{k+1}}+\frac{R^{k-4}}{Z^{k-1}})$, $G_{r\theta}(R,Z)=g^0_{r\theta}(\frac{R^{k-2}}{Z^{k+1}}+\frac{R^{k-4}}{Z^{k-1}})$

For the shear moduli given by

$$G_{\theta z}(R,Z)=g^0_{\theta z}\left(\frac{R^{k-2}}{Z^{k+1}}+\frac{R^{k-4}}{Z^{k-1}}\right),\ G_{r\theta}(R,Z)=g^0_{r\theta}\left(\frac{R^{k-2}}{Z^{k+1}}+\frac{R^{k-4}}{Z^{k-1}}\right), \tag{23}$$

where k is an integer, we obtain from Eq. (12) for ϕ the following

$$\phi=C_0t^k\left[g^0_{r\theta}(k+2)+k(g^0_{r\theta}-g^0_{\theta z})t^2\,{}_2F_1\left(1,\frac{k+2}{2};\frac{k+4}{2};-\frac{g^0_{\theta z}t^2}{g^0_{r\theta}}\right)\right] \tag{24}$$

where constant C_0 is determined by using Eq. (7). The corresponding stresses and the displacement are

$$\tau_{\theta z}=\frac{C_0k(k+2)(g^0_{r\theta})^2t^k(t^2+1)}{L_0^3R^3(g^0_{r\theta}+g^0_{\theta z}t^2)},\ \tau_{r\theta}=\tau_{\theta z}t, \tag{25}$$

$$u_\theta = \frac{C_0 g^0_{r\theta} k(k+2)R}{2g^0_{\theta z} L_0^3} \ln\left(\frac{g^0_{\theta z} t^2 + g^0_{r\theta}}{g^0_{\theta z} t^2 + g^0_{r\theta}(Z_0/Z)^2}\right). \tag{26}$$

We note that for $k(k+2)=0$, the two shear stresses and the tangential displaceement identically vanish.

Variation 4: $G_{\theta z}(R,Z) = g^0_{\theta z}\exp(\eta t^2)$, $G_{r\theta}(R,Z) = g^0_{r\theta}\exp(\eta t^2)$

For

$$G_{\theta z}(R,Z) = g^0_{\theta z}\exp(\eta t^2),\ \ G_{r\theta}(R,Z) = g^0_{r\theta}\exp(\eta t^2) \tag{27}$$

where η is a constant, we solve Eq. (13) to get

$$\phi = \frac{C_0}{{T_1}^{3/2}}\Big[\eta\exp(-T_2)(2\eta g^0_{r\theta} g^0_{\theta z} t^2 - 3(g^0_{\theta z})^2 t^2 + 2\eta(g^0_{r\theta})^2 - 2g^0_{\theta z} g^0_{r\theta}) + \eta c_1 T_1\sqrt{\pi T_2} + c_1 g^0_{\theta z}\sqrt{\pi}\,{T_2}^{3/2}\mathrm{erf}\Big(\sqrt{T_2}\Big)\Big] \tag{28}$$

where $T_1 = g^0_{r\theta} + g^0_{\theta z} t^2$, $T_2 = -\frac{\eta T_1}{g^0_{\theta z}}$, $c_1 = 3g^0_{\theta z} - 2g^0_{r\theta}\eta$, $\mathrm{erf}(z) = \frac{2}{\sqrt{\pi}}\int_0^z e^{-t^2}dt$ is the error function, and constant C_0 is determined from Eq. (7). The corresponding stresses and the displacement are

$$\tau_{\theta z} = \frac{3\eta C_0 (g^0_{\theta z})^3 t^4 \exp(T_1\eta/g^0_{\theta z})}{L_0^3 R^3 (T_1)^{5/2}},\ \tau_{r\theta} = \tau_{\theta z} t, \tag{29}$$

$$u_\theta = \frac{\eta C_0 (g^0_{\theta z})^2 \exp(\eta g^0_{r\theta}/g^0_{\theta z})}{g^0_{r\theta} L_0^2 Z^2}\left[-\frac{t}{(g^0_{r\theta} + g^0_{\theta z} t^2)^{3/2}} + \frac{t}{(g^0_{r\theta}(Z_0/Z)^2 + g^0_{\theta z} t^2)^{3/2}}\right]. \tag{30}$$

We observe from Eqs. (21), (26) and (30) that the circumferential displacement u_θ depends upon the gradation indexes of the shear moduli, is a non-linear function of R and Z, and u_θ/R does not equal a constant. Thus the angle of twist of a circle of radius R on a cross-section $z =$ constant can be controlled by tuning the shear moduli variations.

3.2. Solutions for FGM conical cylinder with curved lateral surfaces

For arbitrarily prescribed spatial variations of $G_{\theta z}(R, Z) > 0$ and $G_{r\theta}(R, Z) > 0$, we cannot analytically solve the problem when the cylinder mantle is bounded by curved surfaces. Here, we use the WRA to numerically solve the problem by taking

$$\phi(R,Z) = \sum_{i=1}^{N} b_i (s)^i, \tag{31}$$

for the stress function. In Eq. (31), the N coefficients $b_i (i = 1, 2, \cdots, N)$ are to be determined, and $s = R/Z^p$ is not non-dimensional. Substitution from Eq. (31) into Eq. (8) gives

$$\tau_{\theta z}(R,Z) = \frac{1}{L_0^3 R^3}\sum_{i=1}^{N} i b_i (s)^i,\ \tau_{r\theta}(R,Z) = \frac{p}{L_0^3 R^2 Z}\sum_{i=1}^{N} i b_i (s)^i = pt\,\tau_{\theta z}(R,Z) \tag{32}$$

We note that boundary conditions (6a) and (6b) are exactly satisfied, and boundary condition (7) requires that

$$\sum_{i=1}^{N} b_i\Big[(\beta_2)^i - (\beta_1)^i\Big] = \frac{M_t}{2\pi} \tag{33}$$

In order to deduce $(N-1)$ linearly independent equations, we substitute for ϕ from Eq. (31) into differential Eq. (12) and get

$$\sum_{i=1}^{N} \psi_i (s)^i b_i = 0 \tag{34}$$

where

$$\psi_i = G_{r\theta}(R,Z)\frac{i(i-4)}{R^2} + G_{\theta z}(R,Z)\frac{ip(ip+1)}{Z^2} + \frac{G_{\theta z}(R,Z)}{G_{r\theta}(R,Z)}\frac{\partial G_{r\theta}(R,Z)}{\partial Z}\left(\frac{ip}{Z}\right) - \frac{G_{r\theta}(R,Z)}{G_{\theta z}(R,Z)}\frac{\partial G_{\theta z}(R,Z)}{\partial R}\left(\frac{i}{R}\right) \tag{35}$$

We multiply both sides of Eq. (34) by the weight function $(s)^j (j = 0, 1, 2, ..., N-2)$, and integrate the resulting equation over the cylinder domain to get the following $(N-1)$ algebraic equations

$$\sum_{i=1}^{N} (X_{ji} b_i) = 0,\ j = 0, 1, 2, \ldots N-2, \tag{36}$$

where $X_{ji} = \int_{z_0}^{L_0} \int_{R_z^i}^{R_z^0} \psi_i s^{i+j} dRdZ$. For known expressions of $G_{\theta z}(R, Z)$ and $G_{r\theta}(R, Z)$, this integral is analytically evaluated by using the Mathematical Software. It can also be numerically evaluated by using a Gauss quadrature rule.

The solution of Eqs. (33) and (36) substituted into Eq. (31) gives the Airy stress function ϕ from which stresses and the displacement are computed.

4. Material tailoring

The material tailoring problem involves finding the shear moduli $G_{\theta z}(R, Z) > 0$ and $G_{r\theta}(R, Z) > 0$ from the following equation

$$\frac{\partial G_{\theta z}(R,Z)}{\partial R}\frac{G_{r\theta}(R,Z)}{G_{\theta z}(R,Z)}\tau_{\theta z} - \frac{\partial G_{r\theta}(R,Z)}{\partial Z}\frac{G_{\theta z}(R,Z)}{G_{r\theta}(R,Z)}\tau_{r\theta} + G_{\theta z}(R,Z)\frac{\partial \tau_{r\theta}}{\partial Z} + G_{r\theta}(R,Z)\left(\frac{\tau_{\theta z}}{R} - \frac{\partial \tau_{\theta z}}{\partial R}\right) = 0 \tag{37}$$

for prescribed spatial variations of the shear stresses $\tau_{\theta z}$ and $\tau_{r\theta}$. As there are two unknown functions in Eq. (37), we assume that the two shear moduli depend upon R and Z through $t = R/Z$ as

$$G_{r\theta}(t) = g(t) G_{\theta z}(t) \tag{38}$$

where $g(t) > 0$ is an arbitrary function of t.

For a FGM conical cylinder with the curved (power-law) lateral surfaces we assume

$$\tau_{\theta z}(R, Z) = \frac{C_i}{R^3}(s)^i \tag{39}$$

where i is an integer, and

$$C_i = \frac{iM_t}{2\pi(\beta_2^i - \beta_1^i)} \tag{40}$$

is determined from boundary condition (7). Substituting from Eq. (39) into equilibrium Eq. (4), and considering boundary conditions (6a) and (6b) on the mantle, we get

$$\tau_{r\theta}(R, Z) = \frac{pC_i}{R^2 Z}(s)^i \tag{41}$$

We note that for $i = 2$ and 3, one of the two non-zero shear stresses is constant on a cross-section $Z =$ constant.

Substituting Eqs. (39) and (41) into Eq. (37), we get

$$\frac{tG_{r\theta}(t)}{G_{\theta z}(t)}\frac{\partial G_{\theta z}(t)}{\partial t} + \frac{pt^3 G_{\theta z}(t)}{G_{r\theta}(t)}\frac{\partial G_{r\theta}(t)}{\partial t} - p(ip+1)t^2 G_{\theta z}(t) - (i-4)G_{r\theta}(t) = 0 \tag{42}$$

that has the solution (recall Eq. (38))

$$G_{\theta z}(t) = G_{\theta z0} \exp\left[\int_{t_0}^{t} H(x)dx\right] \tag{43}$$

where

$$H(x) = \frac{(i-4)[g(x)]^2 + p(ip+1)x^2 g(x) - px^3 g'(x)}{x[px^2 + g(x)]g(x)},$$

and $G_{\theta z0}$ equals the value of $G_{\theta z}$ at the point, $t = t_0$. For an isotropic FGM, we have

$$G_{\theta z}(t) = G_{\theta z0}(pt^2 + 1)^{\frac{ip-i+5}{2}} t^{i-4} \tag{44}$$

Expressions (43) and (44) for the shear modulus $G_{\theta z}$ do not depend upon geometric parameters, β_1, β_2, z_0, L of the cylinder.

5. Example problems

5.1. Accuracy and convergence of the WRA solution for a curved mantle cylinder

Consider an isotropic FGM hollow truncated conical cylinder with parabolic lateral surfaces corresponding to $p = 2$ in Eqs. (1a) and (1b). Values assigned to other geometric parameters and the twisting moment are: $z_0 = 0.5$ m, $L = 0.5$ m, $\beta_1 = 0.5$, $\beta_2 = 1.0$ and $M_t = 2\pi \times 10^3$ KNm. We assume that

$$G(R, Z) = G_0 \exp(t) \tag{45}$$

where G_0 is a reference value of the shear modulus.

For different number of terms in the trial solution values of the shear stress $\tau_{\theta z}$ (in MPa) at the point (0.64, 0.8) are presented in Table 1. It is clear that the stress $\tau_{\theta z}$ has converged for $N = 9$. Henceforth, we take $N = 11$.

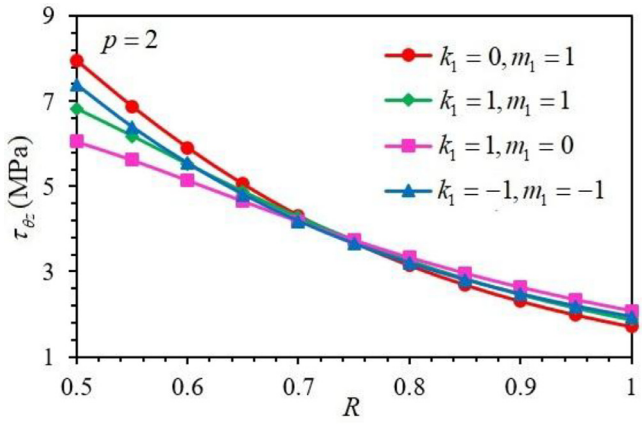

(a) Variation of $\tau_{\theta z}$ on the cross-section $Z = 1.0$

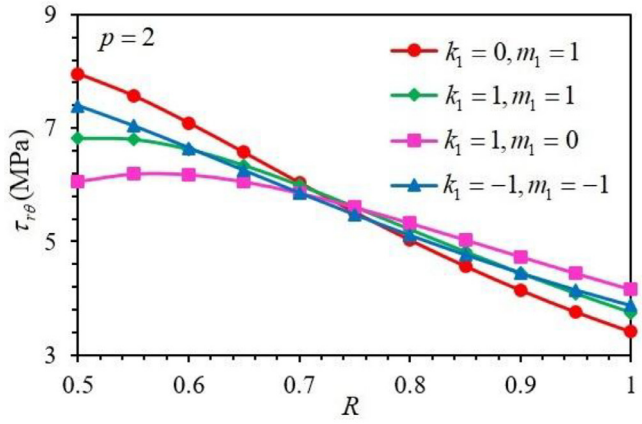

(b) Variation of $\tau_{r\theta}$ on the cross-section $Z = 1.0$

Fig. 2. For $G(R, Z)$ given by Eq. (46), and different values of k_1 and m_1, variations of the two shear stresses with R on the cross-section $Z = 1.0$.

Table 1
Stress $\tau_{\theta z}$ (0.64, 0.8) for different number of terms in the trial function.

Number of terms N	7	9	11	13
$\tau_{\theta z}$	8.4906	8.4914	8.4914	8.4914

Table 2
Comparison of the WRA computed $\tau_{\theta z}$ (R, 0.5) (in MPa) with the exact solution.

R	0.25	0.30	0.35	0.40	0.45	0.50
WRA	8.1736	13.7267	20.2412	27.1681	34.0081	40.3863
Exact	8.1736	13.7267	20.2412	27.1681	34.0081	40.3863

Table 3
Comparison of the WRA computed $\tau_{\theta z}$ (0.5, Z) (in MPa) with the exact solution.

Z	0.60	0.70	0.80	0.90	1.00
WRA	17.0597	7.7326	3.7320	1.9048	1.0217
Exact	17.0597	7.7326	3.7320	1.9048	1.0217

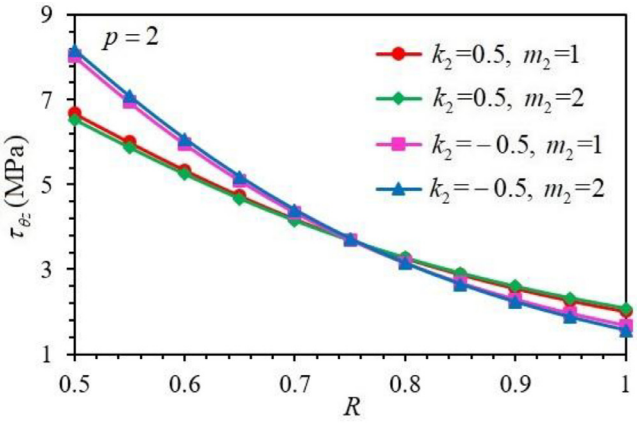

(a) Variation of $\tau_{\theta z}$ on the cross-section $Z = 1.0$

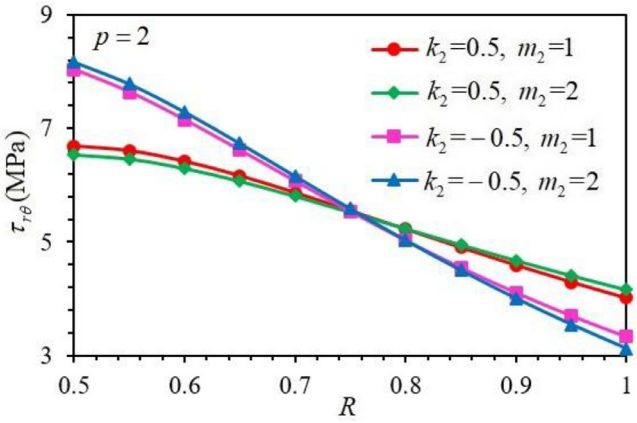

(b) Variation of $\tau_{r\theta}$ on the cross-section $Z = 1.0$

Fig. 3. For $G(R, Z)$ given by Eq. (47) and different values of k_2 and m_2, variations of the two shear stresses with R on the cross-section $Z = 1.0$.

In order to verify accuracy of the numerical solution, we calculate stresses in the cylinder with $p = 1$ (thus $s = t$), and the shear modulus given by Eq. (14) with $g^0_{\theta z} = g^0_{r\theta}$ and $n = 3$. We compare the WRA computed stresses in Tables 2 and 3 with their exact values found from Eq. (16a). The two sets of results exactly agree with each other implying that the WRA with $N = 11$ gives an accurate approximate solution. It is due to the fact that basis functions $(t)^m$, $m = 1, 2,\ldots,11$, provide good approximations of $\frac{t^7}{R^3 g^0_{r\theta}(1+t^2)^{5/2}}$ appearing in Eq. (16a) for $n = 3$.

5.2. Stress distribution

We consider an isotropic FGM hollow cylinder of Section 5.1 and the shear modulus given by

$$G(R, Z) = G_0 R^{k_1} Z^{m_1} \tag{46}$$

$$G(R, Z) = G_0\left[1 + k_2 (t)^{m_2}\right] \tag{47}$$

where G_0 is a reference value of the shear modulus, and k_1, m_1, k_2 and m_2 are constants such that $G(R, Z) > 0$ everywhere in the cylinder domain. We have exhibited in Figs. 2 and 3 the two shear stresses on the cross-section, $Z = 1.0$, for different values of k_1, m_1 and k_2, m_2.

It is observed from Figs. 2 and 3 that the maxima of the shear stresses $\tau_{\theta z}$ occur on the inner surface rather than on the outer surface as is the case for a homogeneous circular cylinder. However, the maxima of $\tau_{r\theta}$ is at a point in the cylinder interior for Eq. (46) describing $G(R, Z)$ and $((k_1, m_1) = (1, 1)$ and $(1,0))$. For $G(R, Z)$ given by Eq. (47), changing the value of k_2 (m_2) from -0.5 to $+0.5$ (1 to 2) greatly (slightly) influences the stress distribution on a cross-section. Thus, one can adjust the maximum shear stress by appropriately varying the shear modulus in the cylinder.

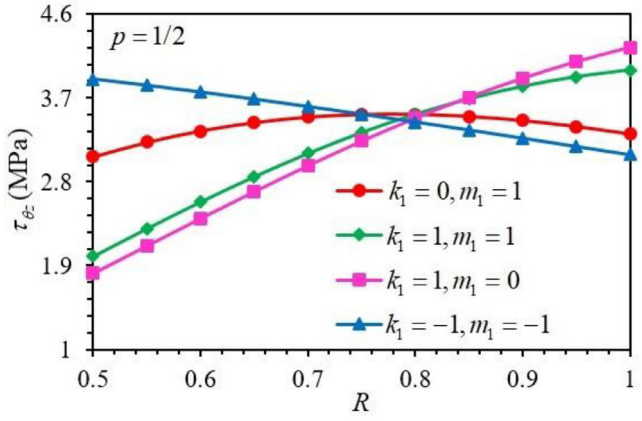

(a) Variation of $\tau_{\theta z}$ on the cross-section $Z = 1.0$

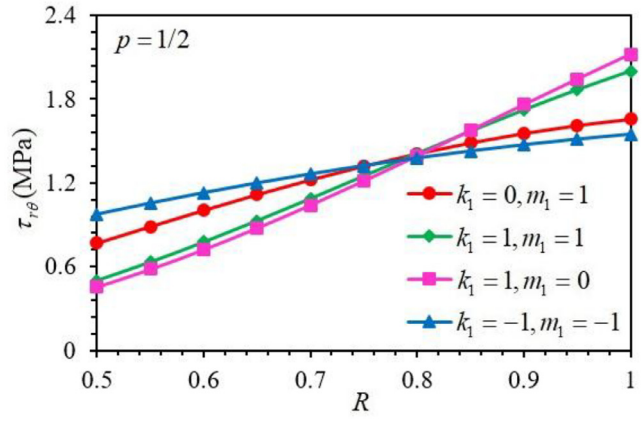

(b) Variation of $\tau_{r\theta}$ on the cross-section $Z = 1.0$

Fig. 4. For $G(R, Z)$ given by Eq. (48), and different values of k_1 and m_1, variations of the two shear stresses with R on the cross-section $Z = 1.0$.

In order to delineate effects of the curvature of the cylinder mantle, we take $p = 1/2$, and

$$G_{\theta z}(R, Z) = G_{\theta z0} R^{k_1} Z^{m_1},\ G_{r\theta}(R, Z) = 1.2 G_{\theta z}(R, Z) \tag{48}$$

for the cylinder studied above. We have displayed in Fig. 4 distributions of the two shear stresses on the cross-section, $Z = 1.0$, for different values of k_1 and m_1. It is clear that the maximum of the shear stress $\tau_{\theta z}$ occurs on the inner surface for $k_1 = m_1 = -1$ and on the outer surface for other values of k_1 and m_1. However, the maximum of the shear stress $\tau_{r\theta}$ is always on the outer surface for the values of k_1 and m_1 considered here. Comparing plots in Figs. 4 and 2, we find that the stress distribution strongly depends upon the mantle geometry, and stresses at a point in the cylinder with $p = 1/2$ are less than those in the cylinder with $p = 2$.

5.3. Material tailoring

5.3.1. Isotropic material

For $i = 2$ and $i = 3$, respectively, in Eqs. (39) and (41), we see that one of the two non-zero shear stresses in the cylinder is constant on a cross-section $Z =$ constant. It holds for all values of p. In the following example problems, we set $L = 0.8$ m, $z_0 = 0.2$ m, and $\alpha_i = \frac{\pi}{10}$, and $\alpha_o = \frac{\pi}{4}$ for the cylinder with $p = 1$.

(a) *Straight lateral surfaces,* i.e., $p = 1$

The required variation of the shear modulus $G_{\theta z} = G_{r\theta}$ deduced from Eq. (44) is

$$G_{\theta z}(R, Z) = G_{\theta z0}(t^2 + 1)^{5/2} t^{-2} \text{ for } i = 2, \tag{49}$$

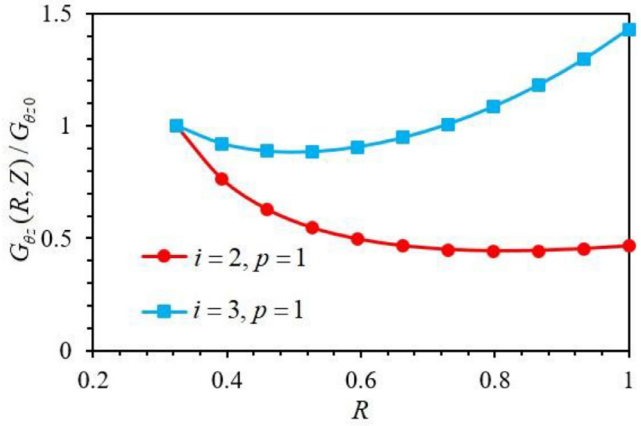

Fig. 5. On the cross-section, $Z = 1.0$, the radial variation of the shear modulus to achieve uniform shear stresses $\tau_{r\theta}$ (for $i = 2,\ p = 1$) and $\tau_{\theta z}$ (for $i = 3,\ p = 1$).

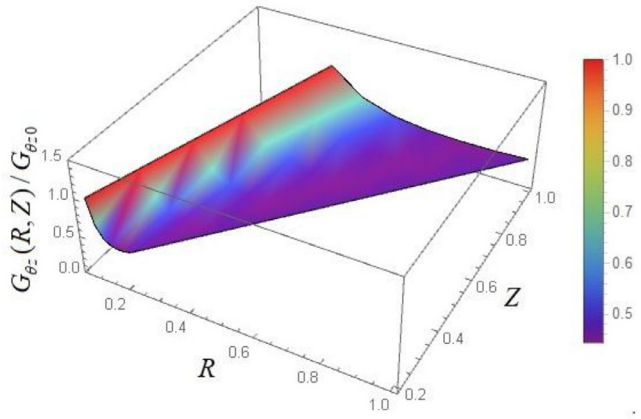

(a) uniform shear stress $\tau_{r\theta}$ ($i = 2, p = 1$)

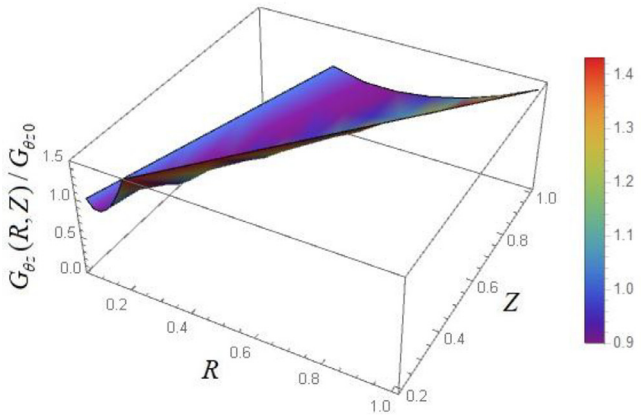

(b) uniform shear stress $\tau_{\theta z}$ ($i = 3, p = 1$)

Fig. 6. The required spatial variation of the shear modulus in the cylinder to achieve uniform shear stress (a) $\tau_{r\theta}$ (for $i = 2,\ p = 1$), and (b) $\tau_{\theta z}$ (for $i = 3,\ p = 1$).

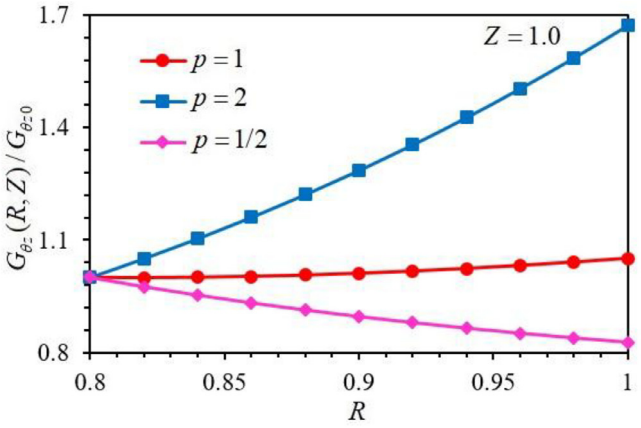

(a) uniform shear stress $\tau_{r\theta}$ ($i = 2$)

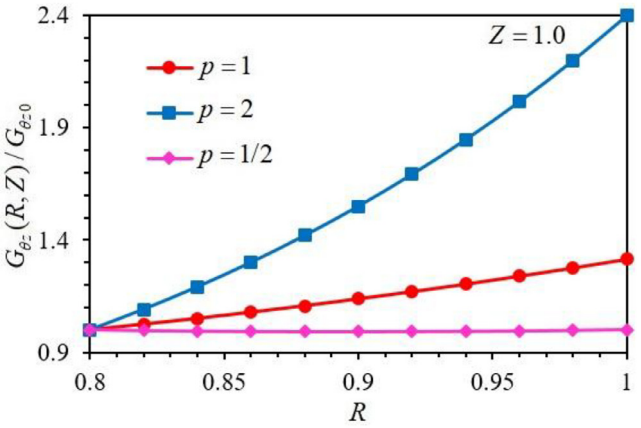

(b) uniform shear stress $\tau_{\theta z}$ ($i = 3$)

Fig. 7. For $p = 1$, 2 and 1/2, the required variation of the shear modulus with R to achieve uniform shear stress (a) $\tau_{r\theta}$ (for $i = 2$), and (b) $\tau_{\theta z}$ (for $i = 3$).

$$G_{\theta z}(R,Z) = G_{\theta z0}(t^2+1)^{5/2}t^{-1} \text{ for } i = 3 \tag{50}$$

Variations with the R- coordinate on the cross-section, $Z = 1.0$, of the shear moduli (49) and (50) are exhibited in Fig. 5. We observe that the shear modulus decreases gradually from the inner to the outer surfaces in order to achieve the uniform shear stress $\tau_{r\theta}$. However, the shear modulus first slowly decreases with an increase in R and then increases to achieve the uniform shear stress $\tau_{\theta z}$ on the cross-section, $Z = 1.0$. For $i = 2$ and $i = 3$, the spatial variations of $G_{\theta z}$ in the cylinder are exhibited in Fig. 6.

(b) *Curved lateral surfaces with* $p = 2$ *and* 1/2

Taking $z_0 = 0.75\,m$, $L = 0.25\,m$, $\beta_1 = 0.8$, $\beta_2 = 1.0$, the results displayed in Fig. 7 for $p = 1$, 2 and 1/2 suggest that the shear modulus increases (decreases) gradually from the inner to the outer surface to achieve either $\tau_{r\theta}$ or $\tau_{\theta z}$ uniform on a cross-section for $p = 1$ and 2 (1/2).

5.3.2. Orthotropic material

(a) *Straight lateral surfaces,* i.e., $p = 1$

In order to investigate the effect of material anisotropy, we have plotted in Fig. 8 for $g(t) = 0.8, 1.0$ and 1.2, the variation of the shear modulus $G_{\theta z}$ with R and Z to achieve the desired shear stress distributions given by Eqs. (39) and (41). We see that the degree of anisotropy signified by the three values assigned to $g(t)$ does not qualitatively affect the spatial variation of the shear moduli but the ratio of their values on the inner and the outer surfaces is noticeably affected. For achieving the uniform shear stress $\tau_{r\theta}$ on a cross-section (see Fig. 8(a)), the ratio of the shear modulus on the outer and the inner surfaces equals 0.65, 0.5 and 0.4, respectively, for $g(t) = 0.8$, 1 and 1.2. However, to achieve the uniform shear stress $\tau_{\theta z}$ on a cross-section (see Fig. 8(b)), this ratio equals 1.8, 1.3 and 1.0, respectively, for $g(t) = 0.8$, 1 and 1.2.

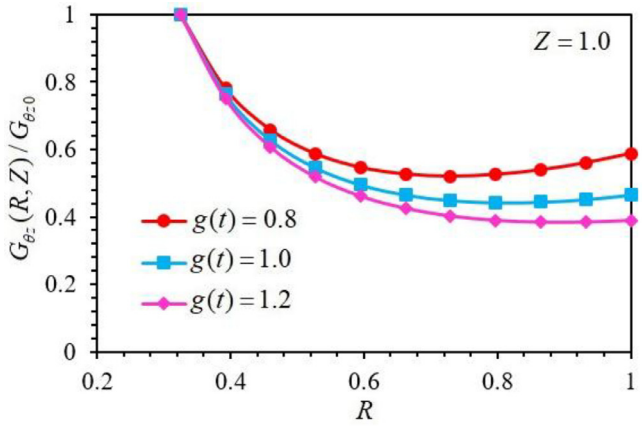

(a) $i=2, p=1$

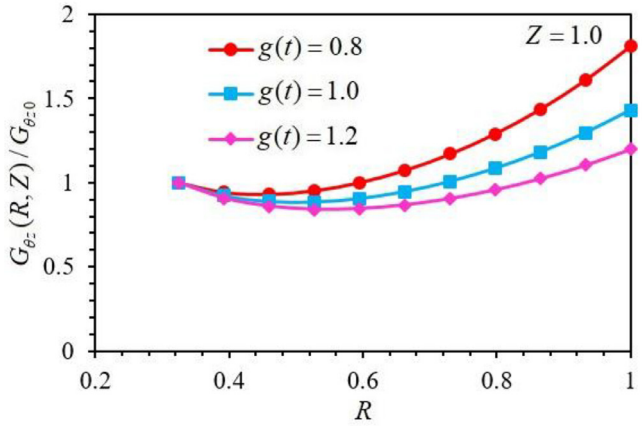

(b) $i=3, p=1$

Fig. 8. For $g(t) = 0.8$, 1 and 1.2, required variations of the shear modulus $G_{\theta z}$ with R to achieve the specified distribution of the stress (a) $\tau_{r\theta}$ (i.e., for $i=2,\ p=1$), and (b) $\tau_{\theta z}$ (i.e., for $i=3,\ p=1$).

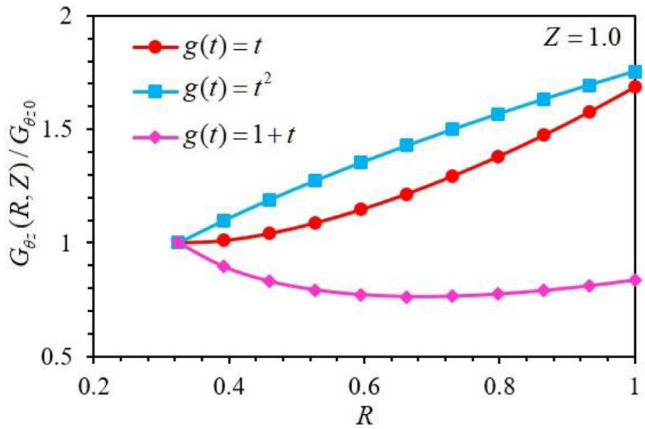

Fig. 9. For $g(t) = t$, t^2 and $1+t$, required variations of the shear modulus $G_{\theta z}$ with R to achieve uniform shear stress $\tau_{\theta z}$ (i.e., for $i=3,\ p=1$) on the cross-section, $Z=1$.

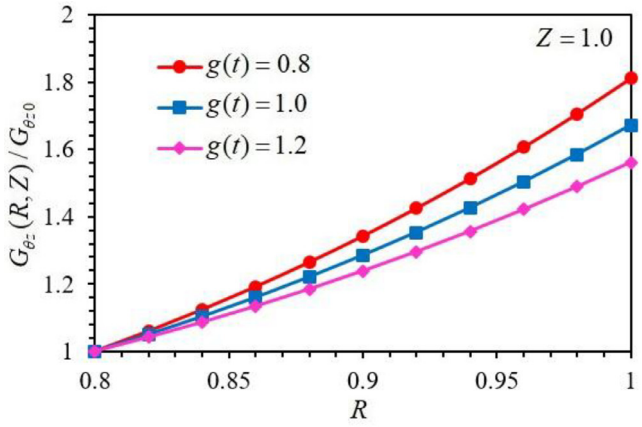

(a) $i = 2, p = 2$

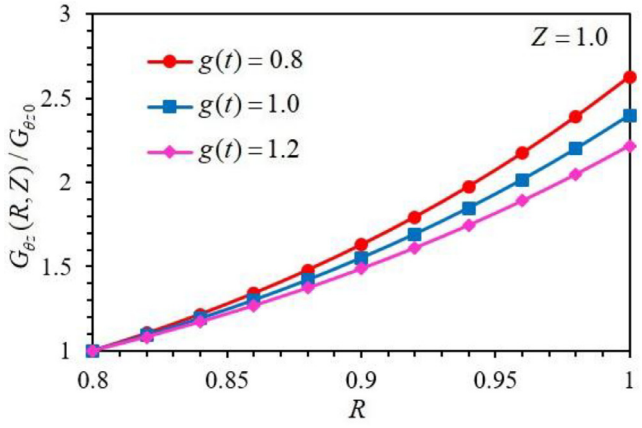

(b) $i = 3, p = 2$

Fig. 10. For $g(t) = 0.8$, 1 and 1.2, required variations of the shear modulus $G_{\theta z}$ with R to achieve uniform shear stress (a) $\tau_{r\theta}$ (i.e., for $i = 2,\ p = 2$), and (b) $\tau_{\theta z}$ (i.e., for $i = 3,\ p = 2$).

We now study the problem for $g(t) = t$, t^2 and $(1 + t)$. The required variations of the shear moduli to achieve the uniform stress $\tau_{\theta z}$ on a cross-section, $Z = 1.0$ are exhibited in Fig. 9. It is clear that for $g(t) = 1 + t$, the required variation of the shear modulus $G_{\theta z}(R, Z)$ decreases from the inner to the outer surfaces but that from the other two expressions it increases with the curvature of the curve depending upon the expression for $g(t)$.

(b) *Curved lateral surfaces with* $p = 2$

We now investigate the effect of material anisotropy on the required variations of the shear moduli to achieve uniform shear stress $\tau_{\theta z}$ or $\tau_{r\theta}$ on a cross-section of the FGM hollow cylinder with curved lateral surfaces described by Eqs. (1a) and (1b) with $p = 2$. Taking $z_0 = 0.75$ m, $L = 0.25$ m, $\beta_1 = 0.8$, $\beta_2 = 1.0$, we have plotted in Fig. 10 for $g(t) = 0.8$, 1.0 and 1.2, the variation of the shear modulus $G_{\theta z}$ with R on a cross-section $Z = 1.0$. Comparing plots in Figs. 10 and 8, we find that the effect of the material anisotropy on results of material tailoring for cylinders with straight and curved lateral surfaces are qualitatively similar to each other. The ratio of the shear moduli on the inner and the outer surfaces increases with a decrease in the value of $g(t)$.

For $g(t) = 0.8$, t and $1 + t$, and $p = 1/2$, $L = 0.8$ m, $z_0 = 0.2$ m, $\beta_1 = 0.325$ and $\beta_2 = 1.0$, the required variations of the shear modulus, $G_{\theta z}(R, Z)$, to achieve the uniform stress $\tau_{\theta z}$ on cross-section, $Z = 1.0$ are depicted in Fig. 11. We see that $G_{\theta z}(R, Z)$ gradually decreases from the inner to the outer surfaces, and the curve for $g(t) = 0.8$ is qualitatively different from those for $g(t) = t$ and $1 + t$.

6. Remarks

We note that equations describing the lateral surfaces strongly influence the form of expressions for the two shear moduli for which the shear stress distributions can be analytically found. The traction-free boundary conditions on the lateral

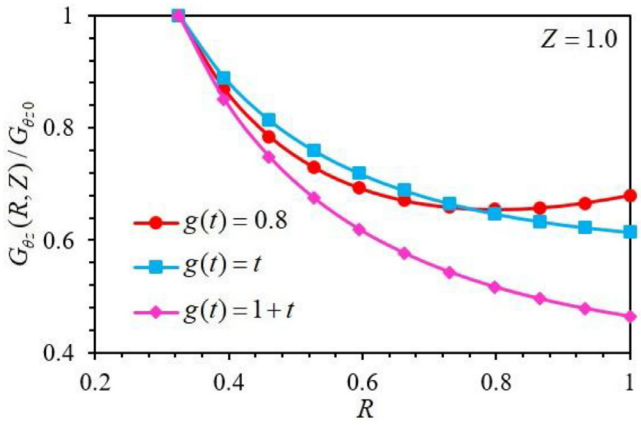

Fig. 11. For $g(t) = 0.8$, t and $1 + t$, required variations of the shear modulus $G_{\theta z}$ with R to achieve the uniform shear stress, $\tau_{\theta z}$ (i.e., for $i = 3,\ p = 1/2$).

surfaces (or the mantle) require that the two non-zero shear stresses satisfy the relation (6a, b) on the cylinder mantle. As pointed out by Lekhnitskii (1962), even for a cone with straight lateral surfaces, the problem has an exact solution only for some specific variations of the two shear moduli.

Recalling the uniqueness theorem for solutions of the linear elasticity equations for the strain energy density positive for non-trivial deformations, the exact solutions derived here are the only ones possible provided that surface tractions and or displacements on the lateral surfaces are exactly satisfied point-wise. However, when only resultant moments and the resultant forces on the end faces equal the prescribed values, as will most likely be the case in test configurations, then according to the St.-Venant principle (e.g., see Batra, 1978; Toupin, 1965), the present solutions are valid at points away from the end faces. In experiments, tangential tractions will very likely be applied on the lateral surfaces near the end faces, as is often the case for the torsion of a straight circular bar. Thus, boundary conditions used here as well as in most continuum problems are somewhat ideal.

We could not find a paper in the open literature listing test results for the torsion of a conical cylinder.

One practical application of a conical cylinder is in coupling two circular shafts of different diameters to transmit torque (or power) between them.

We note that a FGM cylinder can be fabricated by 3-D printing to achieve the desired spatial variation of the two shear moduli.

7. Conclusions

For four variations of the two shear moduli in both the radial and the axial directions, we have derived exact closed-form solutions for the two non-zero shear stresses and the tangential displacement for torsional axisymmetric deformations of an orthotropic FGM hollow truncated conical cylinder with straight lateral surfaces. For a continuous bi-directional variation of the two shear moduli and curved cylinder mantles, we have numerically solved the boundary value problems by using the Weighted Residuals Approach (WRA) whose convergence and accuracy have been established by comparing the numerical and the analytical solutions. We have shown that only 11 terms in the WRA provide a converged and accurate solution of the problems studied. We have also ascertained spatial variation of the two shear moduli for one of two shear stresses to be a constant on a cross-section. The effects of the ratio of the two shear moduli and of the curvature of the lateral surfaces have been illustrated through numerical solutions of example problems.

The analytical solutions provided herein should serve as benchmarks for verifying the convergence and accuracy of numerical solutions. The work can be extended for other spatial variations of the shear moduli and loading scenarios.

Acknowledgments

GJN's work was supported by the National Natural Science Foundation of China grant nos. 11772232, 11372225 and 11072177. RCB's work was partially supported by the US Office of Naval Research grant N000141812548 with Dr. Y. D. S. Rajapakse as the Program Manager. GJN is visiting RCB's research group during the 2018 calendar year.

References

Arghavan, S., & Hematiyan, M. R. (2009). Torsion of functionally graded hollow tubes. *European Journal of Mechanics A/Solids, 28*, 551–559.
Batra, R. C. (1978). Saint-Venant's principle for a helical spring. *Journal of Applied Mechanics, 45*, 297–301.
Batra, R. C. (1980). Finite plane strain deformations of rubberlike materials. *International Journal for Numerical Method Engineering, 15*, 145–160.
Batra, R. C. (2006). Torsion of a functionally graded cylinder. *AIAA Journal, 44*, 1363–1365.

Batra, R. C. (2011). Material tailoring and universal relations for axisymmetric deformations of functionally graded rubberlike cylinders and spheres. *Mathematics and Mechanics of Solids, 16*, 729–738.
Batra, R. C. (2015). Material tailoring in finite torsional deformations of axially graded Mooney-Rivlin circular cylinder. *Mathematics and Mechanics of Solids, 20*, 183–189.
Birman, V., & Byrd, L. W. (2007). Modeling and analysis of functionally graded materials and structures. *Applied Mechanics Reviews, 60*, 195–216.
Chen, T. (2011). A novel class of graded cylinders neutral to host shafts of arbitrary cross-sections under torsion. *Mechanics Research Communications, 38*, 68–71.
Chen, Y. (1964). Torsion of nonhomogeneous bars. *Journal of the Franklin Institute, 277*, 50–54.
Cho, J. R., & Ha, D. Y. (2002a). Optimal tailoring of 2D volume-fraction distributions for heat-resisting functionally graded materials using FDM. *Computer Methods in Applied Mechanics and Engineering, 191*, 3195–3211.
Cho, J. R., & Ha, D. Y. (2002b). Volume fraction optimization for minimizing thermal stress in Ni–Al_2O_3 functionally graded materials. *Materials Science and Engineering A, 334*, 147–155.
Correia, V. M. F., Madeira, J. F. A., Araújo, A. L., & Soares, C. M. M. (2018). Multiobjective optimization of ceramic-metal functionally graded plates using a higher order model. *Composite Structures, 183*, 146–160.
Dryden, J. R., & Batra, R. C. (2013a). Material tailoring and moduli homogenization for finite twisting deformations of functionally graded Mooney-Rivlin hollow cylinders. *Acta Mechanica, 224*, 811–818.
Dryden, J. R., & Batra, R. C. (2013b). Optimum young's modulus of a homogeneous cylinder energetically equivalent to a functionally graded cylinder. *Journal of Elasticity, 110*, 95–110.
Ecsedi, I. (2009). Some analytical solutions for Saint-Venant torsion of non-homogeneous cylindrical bars. *European Journal of Mechanics A/Solids, 28*, 985–990.
Ecsedi, I. (2013). Some analytical solutions for Saint-Venant torsion of non-homogeneous anisotropic cylindrical bars. *Mechanics Research Communications, 52*, 95–100.
Goupee, A. J., & Vel, S. S. (2007). Multi-objective optimization of functionally graded materials with temperature-dependent material properties. *Materials and Design, 28*, 1861–1879.
Gupta, A., & Talha, M. (2015). Recent development in modeling and analysis of functionally graded materials and structures. *Progress in Aerospace Sciences, 79*, 1–14.
Horgan, C. O., & Chan, A. M. (1999). Torsion of functionally graded isotropic linear elastic bars. *Journal of Elasticity, 52*, 181–199.
Huang, J., Fadel, G. M., Blouin, V. Y., & Grujicic, M. (2002). Bi-objective optimization design of functionally gradient materials. *Materials and Design, 23*, 657–666.
Jamshidi, M., & Arghavani, J. (2018). Optimal material tailoring of functionally graded porous beams for buckling and free vibration behaviors. *Mechanics Research Communications, 88*, 19–24.
Jog, C. S., & Mokashi, I. S. (2014). A finite element method for the Saint-Venant torsion and bending problems for prismatic beams. *Computers and Structures, 135*, 62–72.
Katsikadelis, J. T., & Tsiatas, G. C. (2016). Saint-Venant torsion of non-homogeneous anisotropic bars. *Journal of Applied and Computational Mechanics, 2*, 42–53.
Leissa, A. W., & Vagins, M. (1978). The design of orthotropic materials for stress optimization. *International Journal of Solids and Structures, 14*, 517–526.
Lekhnitskii, S. G. (1962). Radial distribution of stresses in the wedge and half-plane with variable modulus of elasticity. *Journal of Applied Mathematics and Mechanics, 26*, 199–206.
Lekhnitskii, S. G. (1981). *Theory of elasticity of an anisotropic body*. Moscow: Mir Publishers.
Liaghat, F., Hematiyan, M. R., & Khosravifard, A. (2014). Material tailoring in functionally graded rods under torsion. *Journal of Mechanical Engineering Science, 228*, 3283–3295.
Lieu, Q. X., & Lee, J. (2017). Modeling and optimization of functionally graded plates under thermo-mechanical load using isogeometric analysis and adaptive hybrid evolutionary firefly algorithm. *Composite Structures, 179*, 89–106.
Na, Kyung-Su, & Kim, Ji-Hwan (2009a). Optimization of volume fractions for functionally graded panels considering stress and critical temperature. *Composite Structures, 89*, 509–516.
Na, Kyung-Su, & Kim, Ji-Hwan (2009b). Volume fraction optimization of functionally graded composite panels for stress reduction and critical temperature. *Finite Elements in Analysis and Design, 45*, 845–851.
Na, Kyung-Su, & Kim, Ji-Hwan (2010). Volume fraction optimization for step-formed functionally graded plates considering stress and critical temperature. *Composite Structures, 92*, 1283–1290.
Nedin, R. D., Vatulyan, A. O., & Bogachev, I. V. (2018). Direct and inverse problems for prestressed functionally graded plates in the framework of the Timoshenko model. *Mathematical Methods in the Applied Sciences, 41*, 1600–1618.
Nie, G. J., & Batra, R. C. (2010a). Exact solutions and material tailoring for functionally graded hollow circular cylinders. *Journal of Elasticity, 99*, 179–201.
Nie, G. J., & Batra, R. C. (2010b). Material tailoring and analysis of functionally graded isotropic and incompressible linear elastic hollow cylinders. *Composite Structures, 92*, 265–274.
Nie, G. J., & Batra, R. C. (2010c). Stress analysis and material tailoring in isotropic linear thermoelastic incompressible functionally graded rotating disks of variable thickness. *Composite Structures, 92*, 720–729.
Nie, G. J., Pydah, A., & Batra, R. C. (2018). Torsion of functionally graded truncated conical cylinders. *Submitted*.
Nie, G. J., Zhong, Z., & Batra, R. C. (2011). Material tailoring for functionally graded hollow cylinders and spheres. *Composites Science and Technology, 71*, 666–673.
Ootao, Y., Kawamura, R., Tanigawa, Y., & Imamura, R. (1999). Optimization of material composition of nonhomogeneous hollow sphere for thermal stress relaxation making use of neural network. *Computer Methods in Applied Mechanics and Engineering, 180*, 185–201.
Ootao, Y., Tanigawa, Y., & Ishimaru, O. (2000). Optimization of material composition of functionally graded plate for thermal stress relaxation using a genetic algorithm. *Journal of Thermal Stresses, 23*, 257–271.
Rooney, F. J., & Ferrari, M. (1995). Torsion and flexure of inhomogeneous elements. *Composites Engineering, 5*, 901–911.
Roque, C. M. C., & Martins, P. A. L. S. (2015). Differential evolution for optimization of functionally graded beams. *Composite Structures, 133*, 1191–1197.
Shabana, Y. M., Elsawaf, A., Khalaf, H., & Khalil, Y. (2017). Stresses minimization in functionally graded cylinders using particle swarm optimization technique. *International Journal of Pressure Vessels and Piping, 154*, 1–10.
Swaminathan, K., & Sangeetha, D. M. (2017). Thermal analysis of FGM plates – A critical review of various modeling techniques and solution methods. *Composite Structures, 160*, 43–60.
Tanaka, K., Watanabe, H., Sugano, Y., & Poterasuc, V. F. (1996). A multicriterial material tailoring of a hollow cylinder in functionally gradient materials: Scheme to global reduction of thermoelastic stresses. *Computer Methods in Applied Mechanics and Engineering, 135*, 369–380.
Toupin, R. A. (1965). Saint-Venant principle. *Archive for Rational Mechanics and Analysis, 18*, 83–96.
Vel, S. S., & Pelletier, J. L. (2007). Multi-objective optimization of functionally graded thick shells for thermal loading. *Composite Structures, 81*, 386–400.
Wang, G., Dong, L., & Atluri, S. N. (2018). Direct and inverse multi-scale analyses of arbitrarily functionally graded layered hollow cylinders (discs), with different shaped reinforcements, under harmonic loads. *Composite Structures, 188*, 425–437.
Wetherhold, R. C., Seelman, S., & Wang, J. (1996). The use of functionally graded materials to eliminate or control thermal deformation. *Composites Science and Technology, 56*, 1099–1104.